

Single-Shot Experimental Localization of Electromagnetic Interference Sources With Application to Electrostatic Discharges

Elias Le Boudec, Hamidreza Karami, David Martinez, Farhad Rachidi, Marcos Rubinstein, and Felix Vega

Abstract – We propose a method to locate the current in a printed circuit board caused by an electrostatic discharge. This approach uses data acquired before the discharge event by using a vector network analyzer. The localization is performed by using single-shot time-domain data and the time-reversal algorithm. The time-reversal backpropagation uses experimental data, eliminating the need for numerical models of the device under test. The method allows us to distinguish two traces placed 8 mm apart.

1. Introduction

Any electronic product must pass electromagnetic compatibility compliance tests before being brought to market. These tests include verifying that the product does not emit noisy radiation due to unintended antennas. On the sensitivity side, products must also be resilient to electrostatic discharges, as specified in IEC 61000-4-2 [1]. When the device under test fails electrostatic discharge tests, it can be challenging to determine which components need to be protected. This requires understanding the path of the discharge current, which can be identified through optical imaging of thermal damage [2]. Near-field scans, the preferred method for electromagnetic interference source imaging [3–5], might be infeasible in this case, because the discharge event and resulting damage are not repeatable. Other approaches include full-wave simulations [6] or coupling modeling by using transfer impedance functions [7].

Manuscript received 25 February 2025. E. L. acknowledges support and funding from the Technology Innovation Institute (agreement TII/DERC/2254/2021).

Elias Le Boudec and Farhad Rachidi are with the Electromagnetic Compatibility Laboratory, EPFL (the Swiss Federal Institute of Technology in Lausanne), Bâtiment ELL, Station 11, 1015 Lausanne, Switzerland; e-mail: elias.leboudec@alumni.epfl.ch, farhad.rachidi@epfl.ch.

Hamidreza Karami and Marcos Rubinstein are with the Institute for Information and Communication Technologies, University of Applied Sciences and Arts Western Switzerland, Route de Cheseaux 1, Case postale, 1401 Yverdon-les-Bains, Switzerland; e-mail: hamidreza.karami@heig-vd.ch, marcos.rubinstein@heig-vd.ch.

David Martinez and Felix Vega are with the Directed Energy Research Center, Technology Innovation Institute, P.O. Box: 9639, Yas Island, Abu Dhabi, United Arab Emirates; e-mail: david.martinez@tii.ae, felix.vega@tii.ae.

The motivation for this work is to provide an imaging method to produce single-shot images of electromagnetic interference, with applications to electrostatic discharges. We propose using the time-reversal method [8]. This method relies on the measurement of radiated fields on a time-reversal mirror (e.g., a single omnidirectional antenna, see [9] for a detailed discussion of time-reversal mirrors). The measurements are then time reversed and propagated back from the time-reversal mirror. Experimental results and theoretical analyses show that the fields converge to the original source location, allowing the image to be produced through various methods [10].

Usually, time-reversal backpropagation is performed numerically [11]. This requires creating a digital twin of both the imaging system and the device under test within the working frequency range. Designing and validating this model is typically time consuming. Therefore, we experimentally perform backpropagation in the presence of the device under test by measuring the transfer functions between the time-reversal mirror and the image plane, located below the device. This image plane corresponds to the physical region in which we can measure the electric field. To our knowledge, this is the first two-dimensional application of time reversal with experimental backpropagation. It offers the advantages of being fast (a few minutes per scan), allowing single-shot experiments, being compatible with a resonant cavity for practical testing, and accounting for field propagation in and around the device itself. We believe this approach is a reasonable path toward a viable commercialization of the method.

2. Methods

The experiments take place in a 1 m³ aluminum resonant cavity, which provides shielding from external interference sources and a high number of modes above the cutoff frequency [12]. An xy linear actuator is used to move a 5 mm monopole antenna in the resonant cavity. The linear actuator, pictured in Figure 1, is designed to mitigate noise and coupling to the motors and controllers and to minimize changes in geometry as the monopole antenna moves. The range of motion of this actuator, a 180 mm by 192.5 mm rectangle, defines the image plane.

The goal of the experiment is to recover the electrostatic discharge current path in a realistic device under test. A custom test printed circuit board (PCB)

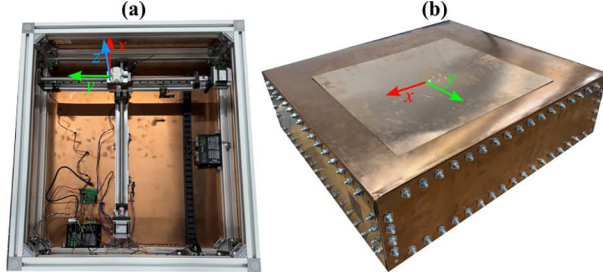


Figure 1. Pictures of the xy linear actuator used to move the scanning monopole antenna: (a) shows the scanner actuators and control and (b) displays the shields and the axes of motion, stemming from the monopole antenna.

was designed (see Figure 2). It consists of pairs of adjacent open-ended traces connected to SMA coaxial connectors. The coaxial shield is connected to the bottom trace and the core to the top trace. In this work, only one trace pair is used, measuring 50 mm in length, with an 8 mm separation. The board is made of FR4, and its thickness is 1.6 mm.

The experiment is in two stages: first, the direct time phase, where unwanted electromagnetic interference is radiated from the custom device under test and recorded on an eight-channel time-reversal mirror (the higher the number of channels, the less sensitive the system is to their positioning, and the lower the noise level; here, we are limited by the number of channels in the RF switch). Schematics of the experiment setup are shown in Figure 3, with pictures in Figure 4. We test two types of excitation signals: a synthetic Gaussian pulse and the current from an electrostatic discharge. The second stage, described in Section 2.3, involves time reversing the measured waveforms and backpropagating them to the image plane to perform source imaging.

In all frequency-domain acquisitions, we work with 4001 samples from 1 GHz to 3 GHz. At lower frequencies, the resonant cavity supports fewer modes, and the imaging resolution degrades because it is proportional to the wavelength. On the other end of the spectrum, the scanner motion starts interfering with the measured fields.

2.1 Synthetic Excitation

Trace $p = 1, 2$ of the device under test is connected to port p of the vector network analyzer (VNA). We measure the scattering parameter from the device under test to

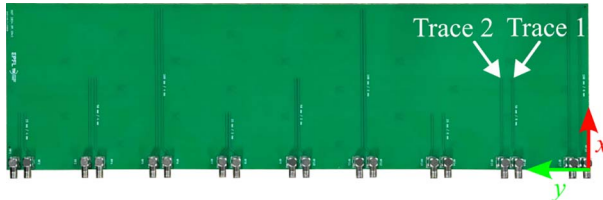


Figure 2. Custom device under test consisting of pairs of adjacent traces of varying separations and lengths. The traces investigated in this article are indicated as traces 1 and 2.

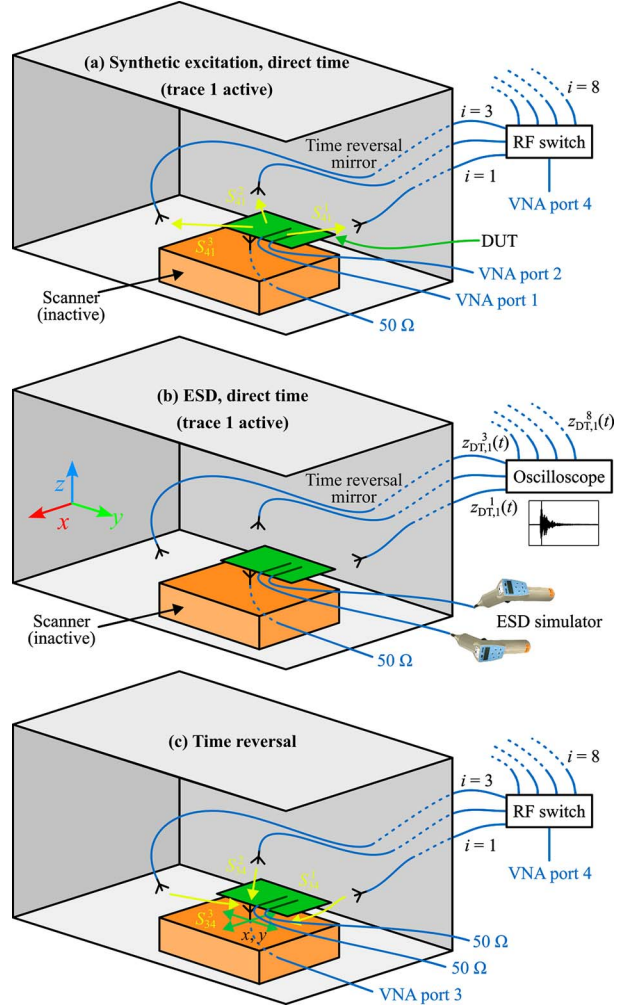


Figure 3. Schematic representation of the experiments. (a) Direct time experiment for the synthetic excitation, (b) direct time experiment for an electrostatic discharge, and (c) time reversal for both excitations.

channel $i = 1, \dots, 8$ of the time-reversal mirror $S_{4,p}^i(f)$ through an RF switch connected to port 4 of the VNA. The synthetic direct time measurements consist of

$$z_{DT,p}^i(f) = S_{4,p}^i(f)g(f) \quad (1)$$

where $g(f)$ is the Fourier transform of a Gaussian pulse

$$g(f) = \frac{1}{2\Delta f} \left[e^{-2\left(\frac{f-f_0}{\Delta f/\pi}\right)^2} + e^{-2\left(\frac{f+f_0}{\Delta f/\pi}\right)^2} \right] \quad (2)$$

and $f_0 = \Delta f = 2$ GHz. This choice focuses most of the energy in the working frequency range of 1 GHz to 3 GHz.

2.2 Electrostatic Discharge

An electrostatic discharge simulator with a 150 pF, 330 Ω discharge network is connected to a target through

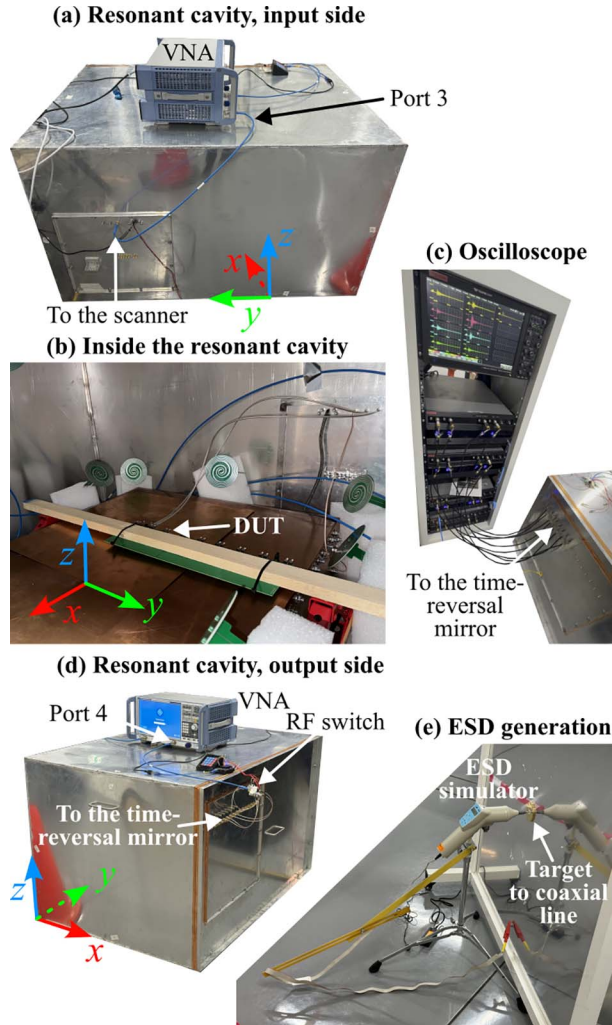


Figure 4. Pictures of the experiment setup. (a) Resonant cavity with port 3 of the VNA connected to the scanner for the time-reversal stage. (b) Inside the resonant cavity, with the cables connecting to VNA ports 1 to 3 connected to coaxial passthroughs. (c) Oscilloscope used to capture time-domain data for the electrostatic discharge excitation. (d) Setup used for the synthetic excitation: port 4 is connected to the time-reversal mirror through an RF switch. (e) Setup used to obtain electrostatic discharges.

a contact discharge electrode, followed by a 20 dB attenuator. A rise time of 0.8 ns and a target peak voltage of 30.6 V were measured according to [1, annex B], with an electrostatic voltage of 4 kV. A coaxial cable then connects the discharge to the device under test. The eight time-reversal channels of the time-reversal mirror are connected to a 16-channel oscilloscope with a sampling rate of 80 GS/s per channel. We thus obtain the direct time time-domain signals $z_{\text{DT},p}^i(t)$, $i = 1, \dots, 8$ when trace $p = 1, 2$ is active. This waveform is transformed to the frequency domain via a fast Fourier transform without windowing (because the measured waveforms have a finite duration, see inset in Figure 3b), and is then multiplied by $g(f)$.

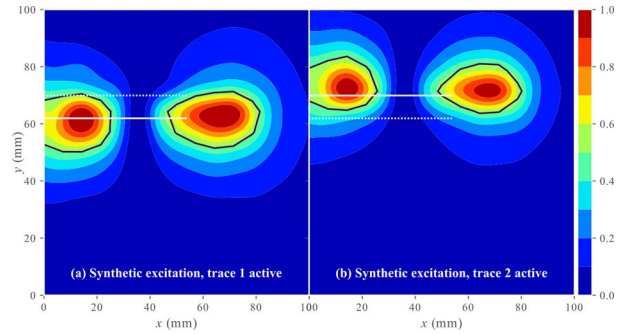


Figure 5. Maximum-normalized absolute value of the time-reversed field $z_{\text{TR},p}(t^*, x, y)$ for the synthetic excitation. (a) Trace 1 active ($p = 1$), (b) trace 2 active ($p = 2$). The horizontal lines indicate the location of the active (solid) and inactive (dashed) traces. The black solid lines indicate the half-maximum isolines.

2.3 Time Reversal

The time-reversal mirror consists of eight PCB-based spiral antennas connected to the VNA through a switch for the synthetic excitation and to the oscilloscope for the electrostatic discharge. Next, we perform time-reversal backpropagation between the time-reversal mirror and the image plane (i.e., the zone of interest). To this end, we measure the transfer function between the time-reversal mirror and the image plane below the device under test by placing the scanning monopole antenna at the position (x, y) and measuring the scattering parameter $S_{3,i}(f, x, y)$ for the time-reversal channel $i = 1, \dots, 8$. Port 3 of the VNA is connected to the scanning monopole antenna. After time reversing the direct time measurements by taking the complex conjugate (denoted by \cdot^*), the time-reversed field in the image plane is

$$z_{\text{TR},p}(f, x, y) = \sum_{i=1}^8 S_{3,i}(f, x, y) [z_{\text{DT},p}^i(f)]^* \quad (3)$$

After taking an inverse Fourier transform to return to the time domain, we select the time slice of maximum absolute value of $z_{\text{TR},p}(t, x, y)$:

$$t^* = \arg \max_t \left[\max_{x,y} |z_{\text{TR},p}(t, x, y)| \right] \quad (4)$$

As mentioned previously, $p = 1, 2$ denotes the active trace in the direct time phase.

3. Results

The spatial distribution of $z_{\text{TR},p}(t^*, x, y)$ is given in Figure 5 for the synthetic excitation and Figure 6 for the electrostatic discharge.

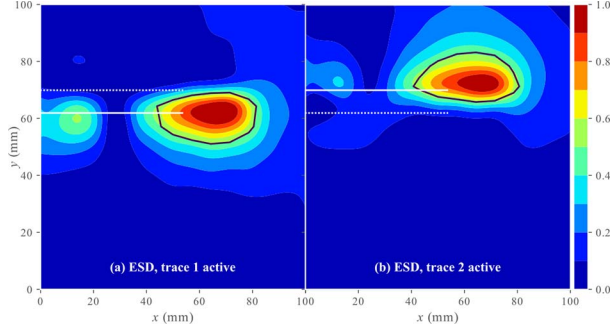


Figure 6. Maximum-normalized absolute value of the time-reversed field $z_{\text{TR},p}(t^*, x, y)$ for the electrostatic discharge and the same layout as Figure 5.

4. Discussion

In all cases, the maximum field amplitude is closest to the active trace, meaning that the proposed method is capable of locating the current responsible for the measured radiated fields. There is a slight increase in focal spot size for electrostatic discharges (Figure 6) caused by the lower signal-to-noise ratio of the time-domain measurement and the lack of control over the frequency band excitation. The shape of the field along the x axis is likely determined by transmission line effects along the length of the trace and a field enhancement at the tip of the traces (explaining the hot spot centered around $x = 70$ mm).

4.1 Imaging Resolution

The obtained full width at half maximum across the y axis is always below 20 mm, which corresponds to $\lambda/7.5$ at the center frequency of 2 GHz. This is better than one might expect in the absence of resolution-enhancing devices such as a resonant metalens [13].

To investigate the subwavelength-focusing capability of the proposed system, we performed a set of numerical simulations by using finite elements in the frequency domain at 1 GHz. The simulation domain is a hemisphere of radius 68.2 cm, with a scattering boundary condition and a metallic bottom plane. The sources consist of two lumped ports enclosed in a metallic coaxial cable feeding two traces with the same geometry as the device under test (a length of 50 mm, a spacing of 8 mm, and a vertical separation of 1.15 mm). The time-reversal mirror consists of eight receiver ports that send back the conjugate of the measured direct time signal in the time-reversal phase. The simulation geometry is depicted in Figure 7.

We study the effect of two parameters: first, the radius $r_{\text{TRM}} \in \{20.99 \text{ cm}, 53.2 \text{ cm}\}$ measured between the center of the device under test and the time-reversal mirror; and second, the angle $\alpha \in \{0^\circ, 30^\circ\}$ formed by the cables. Thus, we study the effect of near- and far-field time-reversal mirrors and the system's sensitivity to

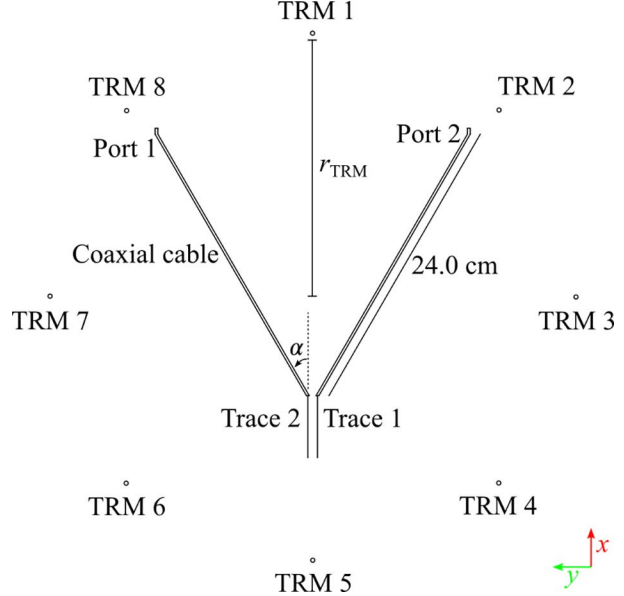


Figure 7. Geometry of the simulation used to determine the effect of the time-reversal mirror and cable placements.

sources with cables at nearby ($\alpha = 0^\circ$) and different ($\alpha = 30^\circ$) locations.

The results in Figure 8 show that the imaging fails for nearby source cables ($\alpha = 0^\circ$) and a far-field time-reversal mirror. When the time-reversal mirror is placed in the near field, the maximum amplitude occurs at the trace coordinates ($x = \pm 4$ mm); however, the image does not distinguish which trace is active. When the source cables are positioned at different locations ($\alpha = 30^\circ$), accurate imaging is achieved with a slightly lower sidelobe level with a near-field time-reversal mirror. In both cases, the imaging resolution is $\sim \lambda/60$.

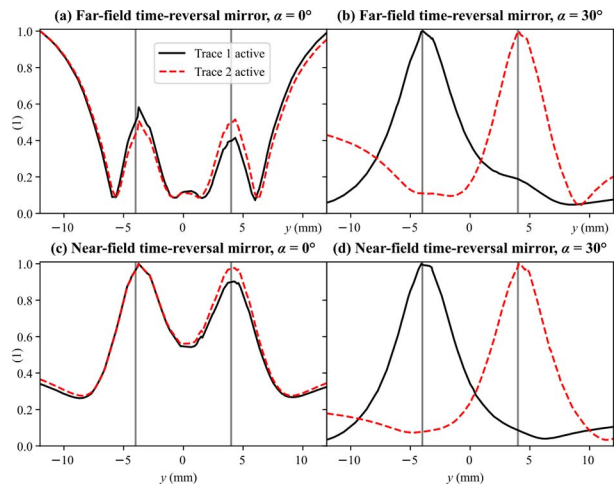


Figure 8. Maximum-normalized norm of the simulated time-reversed electric field when trace 1 or 2 is active. The traces' x coordinates are indicated by the vertical lines. (a) $r_{\text{TRM}} = 53.2$ cm, $\alpha = 0^\circ$, (b) $r_{\text{TRM}} = 53.2$ cm, $\alpha = 30^\circ$, (c) $r_{\text{TRM}} = 20.99$ cm, $\alpha = 0^\circ$, and (d) $r_{\text{TRM}} = 20.99$ cm, $\alpha = 30^\circ$.

Even though this setting is heavily simplified (single frequency, no resonant cavity, simple geometry), it shows that the cable geometry and, to a lesser extent, the near-field coupling between the time-reversal mirror and the source, are responsible for the observed increase in imaging resolution. However, the sensitivity of the resulting resolution, as well as other effects such as bandwidth or resonances, are to be investigated in future work.

5. Conclusion

We have introduced a method to locate the current responsible for unwanted electromagnetic interference radiation and applied it to a synthetic broadband pulse and the single-shot localization of the current path of an electrostatic discharge. The method relies on a mix of frequency- and time-domain data combined with the time-reversal method. We showed that the resolution is sufficient to distinguish the radiation from two traces placed 8 mm apart. Thanks to the use of an indirect experimental backpropagation, there is no need for device or propagation modeling. Furthermore, the results are insensitive to measurement device calibration because the same physical channel is used for the direct time (test) and the backpropagation steps.

Future studies should investigate the case of interference source bandwidths below those of the resonant cavity, which might necessitate mode stirring. Also, resolution-improving devices such as metamaterials may be needed when the cable geometry does not achieve sufficient imaging resolution. Finally, the use of three-dimensional scanning can also be investigated for nonplanar devices under test.

6. Acknowledgments

The authors thank Ali Yaqoob, Islem Yahi, Hamad AlYahyaee, Chaouki Kasmi, and Nicolas Mora for continuing and helpful support during this project.

7. References

1. Electromagnetic compatibility (EMC) – Part 4-2: Testing and measurement techniques – Electrostatic discharge immunity test, IEC 61000-4-2, version 3, IEC Technical Committee 77, Geneva, 2025.
2. S. H. Voldman, *The ESD Handbook*, Hoboken, NJ, Wiley, 2021.
3. H. He, P. Maheshwari, and D. J. Pommerenke, “The Development of an EM-Field Probing System for Manual Near-Field Scanning,” *IEEE Transactions on Electromagnetic Compatibility*, **58**, 2, April 2016, pp. 356-363.
4. S.-W. Guan, C.-W. Kuo, C.-D. Li, and S.-M. Wu, “Multi-directional Trace Current Probe Array Design for Determining ESD Distribution in the Time Domain Through Near-Field Scan,” *IEEE Transactions on Electromagnetic Compatibility*, **62**, 4, August 2020, pp. 987-996.
5. W. Huang, D. Pommerenke, J. Xiao, D. Liu, J. Min, et al., “A Measurement Technique for ESD Current Spreading on a PCB Using Near Field Scanning,” 2009 IEEE International Symposium on Electromagnetic Compatibility, Austin, TX, USA, August 17–21, 2009, pp. 18-23.
6. D. Liu, A. Nandy, F. Zhou, W. Huang, J. Xiao, et al., “Full-Wave Simulation of an Electrostatic Discharge Generator Discharging in Air-Discharge Mode Into a Product,” *IEEE Transactions on Electromagnetic Compatibility*, **53**, 1, February 2011, pp. 28-37.
7. J. Yousaf, J. Shin, K. Kim, J. Youn, D. Lee, et al., “System Level ESD Coupling Analysis Using Coupling Transfer Impedance Function,” *IEEE Transactions on Electromagnetic Compatibility*, **60**, 2, April 2018, pp. 310-321.
8. G. Lerosey, J. de Rosny, A. Tourin, A. Derode, G. Montaldo, et al., “Time Reversal of Electromagnetic Waves,” *Physical Review Letters*, **92**, 19, May 2004, p. 193904.
9. M. Fink and E. Fort, “From the Time-Reversal Mirror to the Instantaneous Time Mirror,” *The European Physical Journal Special Topics*, **226**, 7, May 2017, pp. 1477-1486.
10. E. Le Boudec, H. Karami, N. Mora, F. Rachidi, M. Rubinstein, et al., “Spatiotemporal Energy-Density Distribution of Time-Reversed Electromagnetic Fields,” *IET Science, Measurement & Technology*, **18**, 9, November 2024, pp. 471-482.
11. H. Karami, M. Azadifar, A. Mostajabi, P. Favrat, M. Rubinstein, et al., “Localization of Electromagnetic Interference Sources Using a Time-Reversal Cavity,” *IEEE Transactions on Industrial Electronics*, **68**, 1, January 2021, pp. 654-662.
12. B.-H. Liu and D. C. Chang, *Eigenmodes and the Composite Quality Factor of a Reverberating Chamber*, National Bureau of Standards Technical Note 1066, U.S. Department of Commerce, National Institute of Standards and Technology, Washington, DC, August 1983.
13. F. Lemoult, G. Lerosey, J. de Rosny, and M. Fink, “Resonant Metalenses for Breaking the Diffraction Barrier,” *Physical Review Letters*, **104**, 20, May 2010, p. 203901.